Thermal analysis of porous fins enclosure with the comparison of analytical and numerical methods

S. Hoseinzadeh[1,*], P. S. Heyns[2], A. J. Chamkha[3,4] and A. Shirkhani[5]

Abstract

In this study, heat transfer though a porous fin with rectangular cross section is investigated. The Darcy model is utilized to simulate heat transfer in this porous media. It is assumed that the fin is one-dimensional, homogenous, the flow is laminar, and the generated heat is a linear function of temperature. In this research, three different analytical methods are used to obtain the temperature distribution after deriving the heat transfer equation. In order to validate the obtained solution the collocation method (CM) is compared with the results by a numerical method, in order to validate the solutions, homotopy perturbation method (HPM) and homotopy analysis method (HAM) are employed. This problem is solved for the general case, and the output is obtained as a relationship for one iteration. The effects of various parameters including convection (Nc), porosity (Sh), Rayleigh number (Ra) are examined in this research.

Keywords Porous fin · Darcy model · Dimensionless temperature gradient · CM · HAM · HPM

List of symbols

Ra	Rayleigh number
Sh	Porosity parameter
Nc	Convection parameter
K_r	Ratio of conduction heat transfer
Nr	Radiation parameter
G	Dimensionless number of generated heat
ε	Parameter of internal heat generation
θ	Parameter of surface temperature
Q	Heat transfer rate
α	Thickness ratio
Bi	Biot number
Θ	Dimensionless temperature of convection medium
θs	Dimensionless temperature of sink for radiation
H	Homotopy method

*Correspondence to: S. Hoseinzadeh
hoseinzadeh.siamak@gmail.com

[1] Young Researchers and Elite Club, West Tehran Branch, Islamic Azad University, Tehran, Iran

[2] Centre for Asset Integrity Management, Department of Mechanical and Aeronautical Engineering, University of Pretoria, Pretoria, South Africa

[3] Mechanical Engineering Department, Prince Sultan Endowment for Energy and Environment, Prince Mohammad Bin Fahd University, Al-Khobar 31952, Saudi Arabia

[4] RAK Research and Innovation Center, American University of Ras Al Khaimah, Ras Al Khaimah, United Arab Emirates

[5] School of Chemical, Petroleum and Gas Engineering, Iran University of Science and Technology, Tehran, Iran

Introduction

Porous material [1–3] is a new innovation which provides the ability to gather a specific set of physical, mechanical and biological properties. This has made the aeronautics, car industry, ventilation and electronic industries, industry of medical equipment, constituent parts of the building (concrete, cement, window, solar collector) and especially in nanotechnology, benefit from this novel technology is based on their own requirements [4–27]. Due to the importance of numerical and analytical investigations of heat transfer in fins, various scientists of physics, mathematics and the engineers have focused on this topic. Investigation of extended surface for different cases has been performed based on one- and two-dimensional analyses. Fins are frequently used in various applications of heat transfer. An extensive study has been conducted in this field, and there are numerous references in the field of heat transfer in porous fins.

Chamkha et al. [28–35] proposed a simple method of performance analysis of porous fins in a medium with natural convection. This method was based on energy balance and Darcy's equation for deriving heat transfer

equation. Thermal performance of fin was considered for three types of fins including long, finite length with adiabatic and non-adiabatic ends subjected to specific convection coefficient. In the subsequent sections, it was inferred that the effects of different parameters such as Rayleigh number, Darcy number, ratio of conduction heat transfer K_r and length ratio on temperature distribution along the fin length are incorporated in one parameter called porosity. In addition, the effects of conduction heat transfer ratio and length on heat transfer rate were investigated and compared to solid fin in special condition. Finally, it was indicated that heat transfer rate from porous fin was higher than conventional solid fin. Sheikholeslami and Ganji [17–45] investigated heat transfer (convective–radiative) porous fins with different section shapes and materials. They show that with the increase in porosity, heat transfer from fin was increased. Besides, the results indicated that there is a restriction for the increase in K_r and L/t that affect heat transfer rate from the porous fin. In other research, they utilized Finite Difference Method in order to investigate the performance of different profiles.

Sheikholeslami et al. [46–74] used analytical perturbation method (HAM) and homotopy perturbation method (HPM) and variational iteration method (VIM) to solve equations. In order to evaluate the accuracy of methods, the obtained results were compared to the exact solutions, and it was observed that both mentioned methods were able to solve the vast majority of nonlinear differential equations at high accuracy. They considered rectangular profile for the problem and utilized Darcy model for simulation in porous medium. They used finite difference and combined methods to solve the governing equations. The obtained results indicated that the aluminum porous fin, temperature distribution and heat transfer. Also, they studied heat transfer in a porous fin of various nanofluids and nanoparticles, such as CuO-H_2O and Al_2O_3-H_2O, and investigated the Darcy law for nanofluid flow in a porous cavity under the impact of Lorentz forces and analysis of flow parameter on heat transfer drop for porous fins.

Hoseinzadeh et al. [75–80] studied heat transfer of single/hybrid nanoparticles, hybrid nanofluids, in a differentially heated porous cavity. They analyze the effects of size, shape and type of nanoparticles, type of base fluid and working temperature. Moreover, rectangular, trapezoidal, triangular and parabolic profiles were selected to compare heat transfer rates. Their achievement was a three-dimensional nonlinear equation. For solving the equation, they used Newton–Raphson method. The obtained results revealed that the heat transfer rate (Q) for a profile is a function of length to half of base thickness ratio (α), Biot number (Bi), conduction-radiation number (Nr), dimensionless temperature of convection medium (Θ), and dimensionless temperature of sink for radiation (θs). In addition, they indicated that heat transfer rate for rectangular fins was greater than triangular ones. Finally, by comparing the results of parabolic–concave profile, it was inferred that heat transfer from these fins was the lowest in comparison with the other profiles.

Problem and solving methods

In order to simplify the solution, the following assumptions are prescribed. The rectangular profile which is attached to a vertical wall at constant temperature with laminar and steady flow fin is constructed from a porous, homogenous, isotropic material and saturated by single-phase fluid was considered. The fin and surrounding fluid have constant properties unlike the thermal conductivity. Fin temperature is a function of X, and its variations along Y are neglected. Darcy's law is used to carry out simulation in porous medium, and flow is laminar and steady.

In this study, the fin has adiabatic end with finite length. Linear differential equation defined and it requires two boundary conditions as it is second-order equation [77].

$$\frac{d^2\theta}{dX^2} + 4\mathrm{Rd}\frac{d^2\theta}{dX^2} + G(1 + \varepsilon\theta(X)) - \mathrm{Sh}\theta^2 + (\mathrm{Nc} + \mathrm{Nr})\theta = 0 \tag{1}$$

First boundary condition: $X = 1 \quad \rightarrow \quad \theta(1) = 1$

Second boundary condition: Since fin is adiabatic at the end side, no heat transfer occurs at this side. This is why temperature gradient is zero. Therefore, boundary conditions in dimensionless case will be as follows: $X = 0 \rightarrow \theta'(0) = 1$

Collocation method

In order to provide approximate solutions for nonlinear problems, we can use trial function. For doing this, trial function is usually considered as a function of n specified coefficients including C_1, C_2,… In other words, it is considered as $\mathrm{T.F} = f(c_1, c_2, \ldots, c_n)$. The condition of selecting trial function is as follows: trial function is written as some base functions such as polynomials and trigonometric functions. Trial function is written in a way that it satisfies boundary conditions. Substituting the trial function as the main function causes a residual which is a function of constants and variables. It is desired that residual approaches zero. The constants C_1 to C_s should be determined by a specific method. For doing this, there are several methods including Galerkin and Rayleigh–Ritz Methods.

The Rayleigh–Ritz method includes (n) unknown coefficients, and it provides different situations based on the residual. This method is approximated based on $0 < t < 1$

which is defined in the problem. In this method, the purpose is to find C_1 to C_n in order to determine the residual and trial function as a result. In fact, calculation of trial function will lead us to the final solution. In order to build an approximation for the solution, we select a base function as a polynomial based on X.

$$\begin{aligned}\theta(X) =& 1 + C_1\left(1 - X^2\right) + C_2\left(1 - X^3\right) + C_3\left(1 - X^4\right) \\ &+ C_4\left(1 - X^5\right) + c_5\left(1 - X^6\right) + c_6\left(1 - X^7\right) \\ &+ c_7\left(1 - X^8\right) + c_8\left(1 - X^9\right)\end{aligned} \tag{2}$$

The above approximate solution satisfied the boundary condition. By incorporating Eq. (2) in the differential Eq. (1), the equation of the residual will appear as follows:

$$\begin{aligned}R(X) =& 2\mathrm{Sh}c_1c_4X^5 + 2\mathrm{Sh}c_1c_5X^6 - \mathrm{Sh}c_3^2 - 2\mathrm{Sh}c_1 \\ &- 2\mathrm{Sh}c_2 - 2\mathrm{Sh}c_3 - 2\mathrm{Sh}c_4 - 2\mathrm{Sh}c_5 \\ &- 2\mathrm{Sh}c_6 - 2\mathrm{Sh}c_7 - 2\mathrm{Sh}c_8 - \mathrm{Sh}c_1^2 + \mathrm{Sh}c_2^2 \\ &- \mathrm{Sh}c_4^2 + 2\mathrm{Sh}c_2X^3c_8 - \mathrm{Sh}c_5^2 - \mathrm{Sh}c_6^2 - \mathrm{Sh}c_7^2 \\ &- \mathrm{Nc}c_2 - \mathrm{Nc}c_3 - \mathrm{Nc}c_4 - \mathrm{Nc}c_5 - \mathrm{Nc}c_6 \\ &- \mathrm{Nc}c_7 - \mathrm{Nc}c_8 - \mathrm{Nr}c_1 - \mathrm{Nr}c_2 - \mathrm{Nr}c_3 - \mathrm{Nr}c_4 \\ &- \mathrm{Nr}c_5 - \mathrm{Nr}c_6 - \mathrm{Nr}c_7 - \mathrm{Nr}c_8 - 2\mathrm{Sh}c_1X^9c_6 \\ &+ 2\mathrm{Sh}c_1X^2c_7 - 2\mathrm{Sh}c_1X^{10}c_7 + 2\mathrm{Sh}c_1X^2c_8 \\ &- 2\mathrm{Sh}c_1X^{11}c_8 + \cdots + 2\mathrm{Sh}c_2c_3X^4 + 2\mathrm{Sh}c_2c_4X^5 \\ &+ 2\mathrm{Sh}c_2c_5X^6 + 2\mathrm{Sh}c_2c_6X^7 + 2\mathrm{Sh}c_2c_7X^8 \\ &+ 2\mathrm{Sh}c_2c_8X^9 + 2\mathrm{Sh}c_2X^3c_3 2\mathrm{Sh}c_2X^3c_6 \\ &- 2\mathrm{Sh}c_2X^{10}c_6 + 2\mathrm{Sh}c_2X^3c_7 - 2\mathrm{Sh}c_2X^{11}c_7 \\ &- 2\mathrm{Sh}c_2X^{12}c_8 + 2\mathrm{Sh}_3c_4X^5 + 2\mathrm{Sh}c_3c_5X^6 \\ &+ 2\mathrm{Sh}c_3c_6X^7 + 2\mathrm{Sh}c_3c_7X^8 + 2\mathrm{Sh}c_3c_8X^9 \\ &+ 2\mathrm{Sh}c_3X^4c_4 - 2\mathrm{Sh}c_3X^9c_4 - 2\mathrm{Sh}c_6X^{16}c_8 \\ &+ 2\mathrm{Sh}c_7c_8X^9 + 2\mathrm{Sh}c_7X^8c_8 - 2\mathrm{Sh}c_7X^{17}c_8 \\ &- \mathrm{Nc} - \mathrm{Nr} - 288Rdc_8X^7 - 24Rdc_2X \\ &- 120Rdc_5X^4 - 168Rdc_6X^5 - 48Rdc_3X^2 \\ &- 80Rdc_4X^3 - \mathrm{Sh}c_8^2 - \mathrm{Nc}c_1 - 224Rdc_7X^6 \\ &+ 2\mathrm{Sh}c_2^2X^3 - 2\mathrm{Sh}c_2c_3 - \mathrm{Sh} = 0\end{aligned} \tag{3}$$

For obtaining the constant coefficients C_1 to C_n in the range of $0 < X < 1$, we have:

$$\begin{aligned}&R\left(\frac{1}{9}\right) = 0, \quad R\left(\frac{2}{9}\right) = 0, \quad R\left(\frac{3}{9}\right) = 0, \quad R\left(\frac{4}{9}\right) = 0, \\ &R\left(\frac{5}{9}\right) = 0, \quad R\left(\frac{6}{9}\right) = 0, \quad R\left(\frac{7}{9}\right) = 0, \quad R\left(\frac{8}{9}\right) = 0\end{aligned} \tag{4}$$

By solving the above equations, the coefficients $C_1, C_2, C_3, C_4, C_5, C_6, C_7$ and C_8 can be calculated based on different values of Sh, Nc, Nr, Rd.

Homotopy Method

In this section, homotopy method $H(\tau)$ is used to solve Eq. (1) based on the boundary conditions (6).

$$\begin{aligned}H(\theta, p) =& (1 - P)[\theta''(X) - \theta(X) - g_0(X)] \\ &+ p\Big[\theta''(X) + 4Rd\theta''(X) - \mathrm{Sh}\theta''(X)^2 \\ &+ G(1 + \varepsilon\theta(X)) + (\mathrm{Nc} + \mathrm{Nr})\theta(X)] = 0,\end{aligned} \tag{5}$$

where P is the defined parameter in the range of $P \in [0, 1]$. For $P = 0$ and $P = 1$ we have:

$$\theta(X, 0) = \theta_0(X), \quad \theta(X, 1) = \theta(X) \tag{6}$$

Therefore, when P increases from 0 to 1, $\theta(X; p)$ changes from $\theta_0(X)$ to $\theta(X)$.

$$\begin{aligned}\theta(X) &= \theta_0(X) + p\theta_1(X) + p^2\theta_2(X) + \cdots \\ &= \sum_{i=0}^{n} p^i\theta_i(X), \ g_0 = 0\end{aligned} \tag{7}$$

By substituting in Eq. (2) and rearranging the results based on the power of P ($M = 1, \ \beta = -0.4$ for example)

$$\begin{aligned}&P^0 : (1 + 4Rd)\theta_0''(X) = 0 \\ &\theta_0(1) = 1, \theta_0'(0) = 0\end{aligned} \tag{8}$$

$$\begin{aligned}&P^1 : \theta_1''(X) - \mathrm{Sh}\theta_0(X)^2 - \mathrm{Nr}\theta_0(X) - \mathrm{Nc}\theta_0(X) \\ &+ 4Rd\theta_1''(X) + G + G\varepsilon\theta_0(X) = 0 \\ &\theta_1(1) = 0, \ \theta_1'(0) = 0\end{aligned} \tag{9}$$

$$\begin{aligned}&p^2 : 4Rd\theta_2''(X) - \mathrm{Nr}\theta_1(X) - \mathrm{Nc}\theta_1(X) + \theta_2''(X) \\ &- 2\mathrm{Sh}\theta_0(X)\theta_1(X) + G\varepsilon\theta_1(X) = 0 \\ &\theta_2(1) = 0, \ \theta_2'(0) = 0\end{aligned} \tag{10}$$

$$\begin{aligned}&p^3 : \theta_3''(X) - \mathrm{Nc}\theta_2(X) + 4Rd\theta_3''(X) - \mathrm{Nr}\theta_2(X) \\ &- 2\mathrm{Sh}\theta_0(X)\theta_2(X) - \mathrm{Sh}\theta_1(X)^2 + G\varepsilon\theta_2(X) = 0 \\ &\theta_3(1) = 0, \theta_3'(0) = 0\end{aligned} \tag{11}$$

$\vdots$

From Eq. (10) with the boundary conditions, we have:

$$\theta_0(X) = 1 \tag{12}$$

$$\begin{aligned}\theta_1(X) =& \frac{1}{2}\frac{(-G + \mathrm{Nc} + \mathrm{Nr} + \mathrm{Sh} - G\varepsilon)X^2}{1 + 4Rd} \\ &+ \frac{1}{2}\frac{G - \mathrm{Nc} - \mathrm{Nr} - \mathrm{Sh} + G\varepsilon}{1 + 4Rd}\end{aligned} \tag{13}$$

$$\theta_2(X) = \frac{1}{2}\frac{(G - \mathrm{Nc} - \mathrm{Nr} - \mathrm{Sh} + G\varepsilon)(-\mathrm{Nc} - \mathrm{Nr} - 2\mathrm{Sh} + G\varepsilon)}{(1+4Rd)^2} \times \frac{1}{2}\left(\frac{1}{12}x^4 - \frac{1}{2}x^2\right) + \frac{5}{24(1+8Rd+16Rd^2)} \times \left[G^2\varepsilon^2 + 3\mathrm{ShNr} - 2\mathrm{Nc}G\varepsilon - \mathrm{Nc}G + 2\mathrm{NcNr} - 2G\varepsilon\mathrm{Nr}G^2\varepsilon + 2\mathrm{Sh}^2 - 3G\varepsilon\mathrm{Sh} - 2\mathrm{Sh}G + \mathrm{Nr}^2 - \mathrm{Nr}G + \mathrm{Nc}^2 + 3\mathrm{NcSh}\right]$$

$$\vdots \tag{14}$$

Finally, by solving the equation when $p \to 1$, we will have:

$$\theta(X) = \sum_{i=0}^{N} \mathrm{Lim}_{p\to 1} p^{\mathrm{i}}\theta_{\mathrm{i}}(X) \tag{15}$$

Results

Comparison between different solving methods

In the curves provided in Fig. 1, comparison between different methods including collocation method (CM), homotopy perturbation method (HPM) and homotopy analysis method (HAM) with the numerical Runge–Kutta method for different values of Nc, Nr, Rd and Sh with the results of numerical method for boundary value problems. Results indicate that the mentioned methods are so strong in solving the present problem. Also, Table 1 indicates the results obtained by analytical method and numerical method for boundary value problems. Table 2 indicates the results obtained by analytical method and numerical method for boundary value problems.

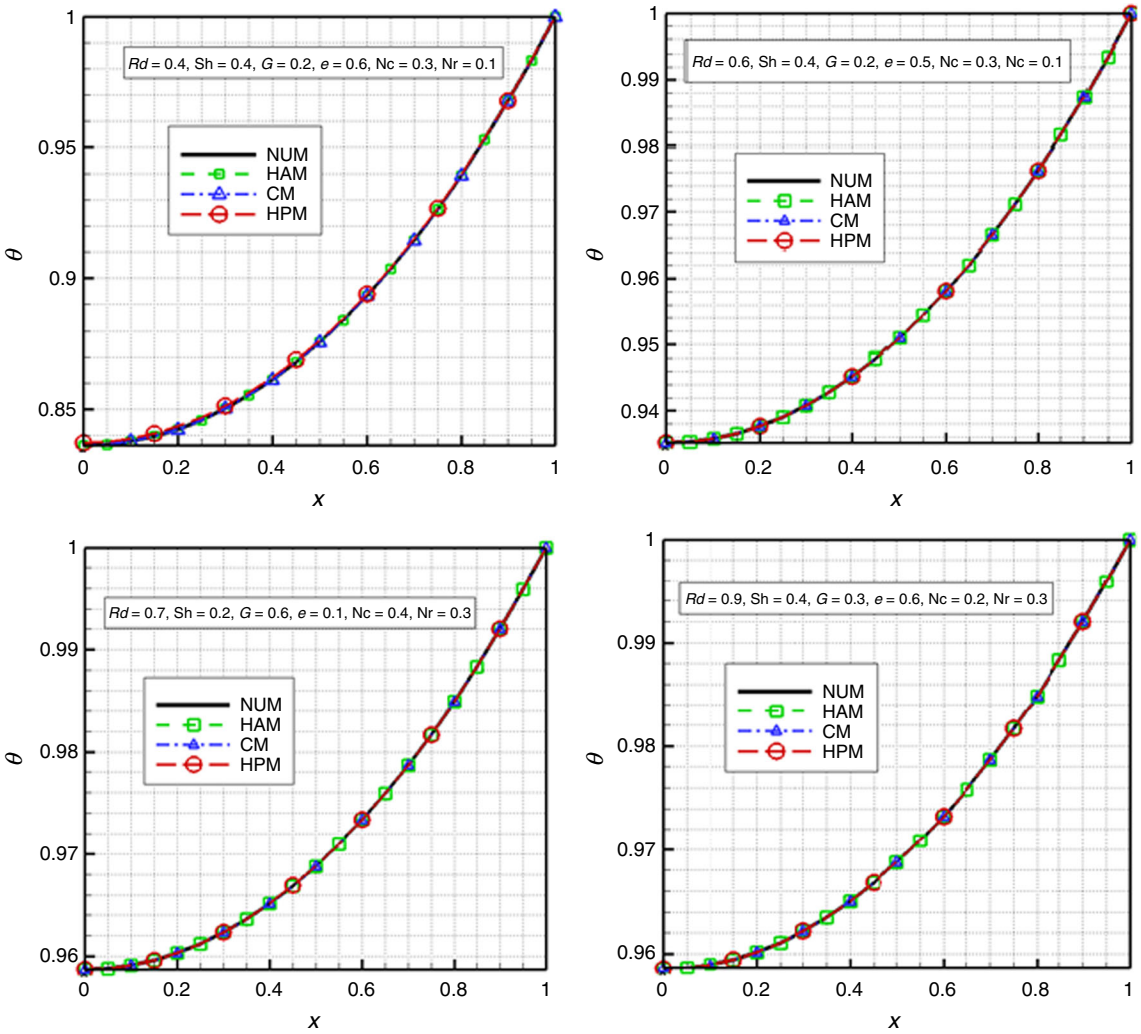

Fig. 1 Comparison between different methods including collocation, homotopy perturbation and homotopy analysis methods with the numerical Runge–Kutta method

Table 1 Comparison of numerical and analytical methods of HAM, CM and HPM for $Rd = 0.6, \mathrm{Sh} = 0.4, G = 0, \mathrm{Nc} = 0.3, \mathrm{Nr} = 0.1$

X	HAM	CM	HPM	Num.	Error of HAM	Error of CM	Error of HPM
0.00	0.897079121	0.89707909	0.897077821	0.897079127	5.90E−09	3.62000E−08	1.3053E−06
0.05	0.897329407	0.897329377	0.897328112	0.897329391	1.58E−08	1.44477E−08	1.2794E−06
0.10	0.898080472	0.898080441	0.898079189	0.898080471	1.00E−09	2.94474E−08	1.2819E−06
0.15	0.899332932	0.899332901	0.89933167	0.899332937	4.90E−09	3.54890E−08	1.2674E−06
0.20	0.901087819	0.901087788	0.901086585	0.901087821	2.00E−09	3.28237E−08	1.2361E−06
0.25	0.903346578	0.903346547	0.90334538	0.903346581	2.20E−09	3.32047E−08	1.2002E−06
0.30	0.906111073	0.906111042	0.906109919	0.906111076	2.40E−09	3.36356E−08	1.1569E−06
0.35	0.909383588	0.909383557	0.909382484	0.909383589	4.00E−10	3.19209E−08	1.1044E−06
0.40	0.913166834	0.913166802	0.913165787	0.913166833	1.00E−09	3.06023E−08	1.0456E−06
0.45	0.917463951	0.917463919	0.917462968	0.91746395	1.60E−09	3.01716E−08	9.8163E−07
0.50	0.922278518	0.922278486	0.922277604	0.922278514	4.20E−09	2.74392E−08	9.0967E−07
0.55	0.927614557	0.927614525	0.927613717	0.927614551	5.40E−09	2.59427E−08	8.3383E−07
0.60	0.93347654	0.933476509	0.93347578	0.933476535	5.30E−09	2.54704E−08	7.5445E−07
0.65	0.939869402	0.939869372	0.939868726	0.939869395	6.90E−09	2.27767E−08	6.6885E−07
0.70	0.946798546	0.946798518	0.946797958	0.946798537	8.60E−09	1.96598E−08	5.7939E−07
0.75	0.954269855	0.954269829	0.954269358	0.954269849	6.60E−09	1.96715E−08	4.9021E−07
0.80	0.962289706	0.962289683	0.962289304	0.962289701	5.50E−09	1.78223E−08	3.9685E−07
0.85	0.970864979	0.970864959	0.970864674	0.970864971	8.50E−09	1.12455E−08	2.9697E−07
0.90	0.980003073	0.980003058	0.980002867	0.980003079	6.20E−09	2.07769E−08	2.1193E−07
0.95	0.989711919	0.989711911	0.989711815	0.989711953	3.38E−08	4.20042E−08	1.3776E−07
1.00	1.000000000	1.000000000	1.000000000	1.000000000	0.000000	0.000000000	0.00000000

Table 2 Comparison of numerical and analytical methods HAM, CM and HPM for $Rd = 0.7, \mathrm{Sh} = 0.2, G = 0, \mathrm{Nc} = 0.4, \mathrm{Nr} = 0.3$

X	HAM	CM	HPM	Num.	Error of HAM	Error of CM	Error of HPM
0.00	0.894162789	0.894162788	0.894162588	0.894162814	2.52E−08	2.56000E−08	2.26400E−07
0.05	0.894421297	0.894421297	0.894421096	0.894421308	1.06E−08	1.09979E−08	2.11144E−07
0.10	0.895197002	0.895197001	0.895196803	0.895197022	2.07E−08	2.10835E−08	2.19276E−07
0.15	0.896490442	0.896490442	0.896490247	0.896490467	2.46E−08	2.51057E−08	2.20063E−07
0.20	0.898302520	0.898302520	0.898302329	0.898302543	2.28E−08	2.32777E−08	2.13745E−07
0.25	0.900634497	0.900634497	0.900634312	0.900634520	2.29E−08	2.34202E−08	2.08180E−07
0.30	0.903488000	0.903488000	0.903487822	0.903488023	2.32E−08	2.36377E−08	2.01520E−07
0.35	0.906865021	0.906865020	0.906864850	0.906865042	2.17E−08	2.24257E−08	1.92318E−07
0.40	0.910767918	0.910767917	0.910767757	0.910767939	2.09E−08	2.15027E−08	1.82354E−07
0.45	0.915199424	0.915199423	0.915199272	0.915199444	2.04E−08	2.10612E−08	1.71894E−07
0.50	0.920162644	0.920162643	0.920162503	0.920162662	1.85E−08	1.92320E−08	1.59144E−07
0.55	0.925661063	0.925661062	0.925660934	0.925661080	1.73E−08	1.80507E−08	1.46224E−07
0.60	0.931698548	0.931698547	0.931698432	0.931698565	1.67E−08	1.76202E−08	1.33320E−07
0.65	0.938279357	0.938279356	0.938279254	0.938279372	1.51E−08	1.57571E−08	1.18338E−07
0.70	0.945408140	0.945408139	0.945408050	0.945408152	1.27E−08	1.35093E−08	1.02414E−07
0.75	0.953089946	0.953089945	0.953089871	0.953089959	1.25E−08	1.34341E−08	8.81937E−08
0.80	0.961330234	0.961330233	0.961330173	0.961330245	1.13E−08	1.21201E−08	7.23534E−08
0.85	0.970134874	0.970134873	0.970134828	0.970134881	7.00E−09	7.63790E−09	5.30487E−08
0.90	0.979510159	0.979510159	0.979510129	0.979510173	1.33E−08	1.37031E−08	4.40762E−08
0.95	0.989462814	0.989462814	0.989462798	0.989462841	2.73E−08	2.76311E−08	4.28286E−08
1.00	1.000000000	1.000000000	1.000000000	1.000000000	0.000000	0.000000000	0.000000000

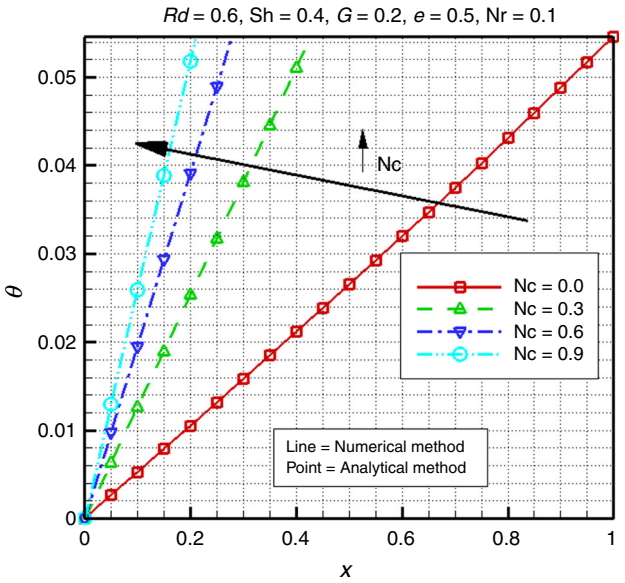

Fig. 2 Dimensionless temperature gradient versus Nc

The effect of different parameters on temperature gradient

In Fig. 2, the effect of changing convention parameter on dimensionless temperature gradient versus fin length is illustrated. According to these variations, it can be inferred that with the increase in different parameters such as convection, temperature gradient along fin is increased. As a result, temperature difference between fin and surroundings will be greater, and great transfer from the surface will take place more easily, which decreases the slope of variations. Besides, in order to investigate the effect of radiation-surroundings parameter, dimensionless temperature gradient based on dimensionless length for different values of Nr is provided in Fig. 3.

According to these variations, it can be inferred that with the increase in radiation-surroundings parameter, temperature gradient increases along the fin length. As a result, temperature difference between fin and surroundings will be greater, and great heat transfer from the surface will take place more easily. Besides, dimensionless temperature gradient based on dimensionless length for different values of Sh is provided in Fig. 4.

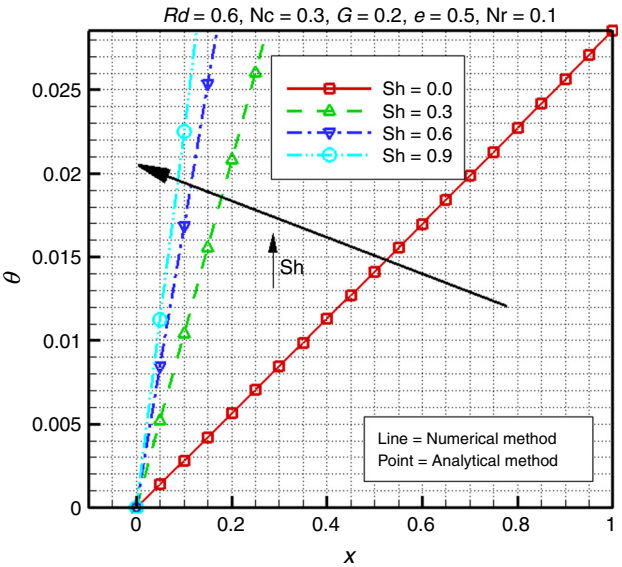

Fig. 4 Dimensionless temperature gradient for different values of Sh

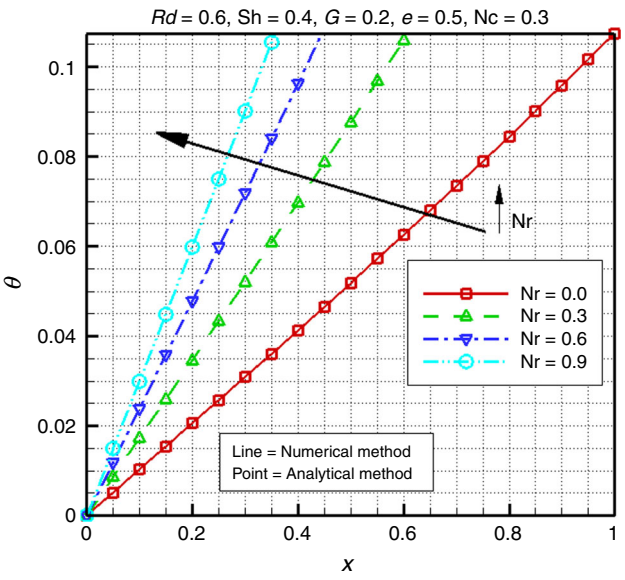

Fig. 3 Dimensionless temperature gradient based on different Nr

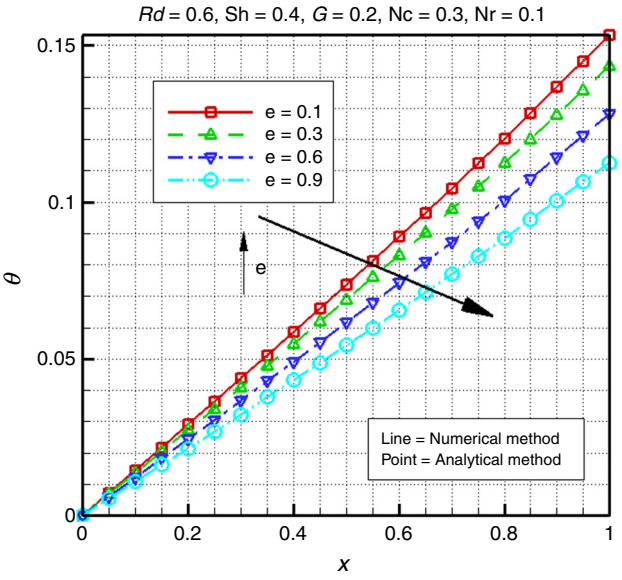

Fig. 5 Dimensionless temperature gradient for different values of *e*

As illustrated in Figs. 4 and 5, it can be inferred that with the increase in porosity parameter and decrease in internal heat generation parameter, temperature gradient increases along the fin length. As a result, temperature difference between fin and surroundings will be greater, and great heat transfer from the surface will take place more easily. Besides, comparison between the obtained profiles reveals that the radiation-surroundings parameter has more significant impact compared to convection parameter.

Conclusions

In this research, the application of the homotopy analysis method (HAM), homotopy perturbation method (HPM) and collocation method (CM), and validation of their applications in heat transfer problems was studied and compared with themselves. Also, nonlinear equation of temperature along with deriving process of the temperature gradient and the effects of various parameters have been investigated and the following conclusions have been obtained:

- With the increase in some parameters including porosity, convection and radiation-surroundings, the temperature gradient along the fin length rises. Consequently, the temperature difference between the fin and surroundings becomes greater. This simplifies the heat transfer from the surface.
- Comparison between the temperature profiles reveals that the radiation parameters have more considerable impact on the temperature distribution in comparison with the convection parameters.
- With the increase convection, porosity, and radiation-surroundings parameters, the heat flow is increased from ($x = 1$).

References

1. Sheikholeslami M, Sajjadi H, Amiri Delouei A, et al. Magnetic force and radiation influences on nanofluid transportation through a permeable media considering Al_2O_3 nanoparticles. J Therm Anal Calorim. 2018. https://doi.org/10.1007/s10973-018-7866-7.
2. Keshavarz F, Mirabdolah Lavasani A, Bayat H. Numerical analysis of effect of nanofluid and fin distribution density on thermal and hydraulic performance of a heat sink with drop-shaped micropin fins. J Therm Anal Calorim. 2018. https://doi.org/10.1007/s10973-018-7093-2.
3. Sheikholeslami M, Jafaryar M, Shafee A, et al. Nanofluid heat transfer and entropy generation through a heat exchanger considering a new turbulator and CuO nanoparticles. J Therm Anal Calorim. 2018. https://doi.org/10.1007/s10973-018-7866-7.
4. Szilágyi IM, et al. WO3photocatalysts: influence of structure and composition. J Catal. 2012;294:119–27.
5. Szilágyi IM, et al. Stability and controlled composition of hexagonal WO_3. Chem Mater. 2008;20:4116–25.
6. Szilagyi IM, et al. Gas sensing selectivity of hexagonal and monoclinic WO3 to H2S. Solid State Sci. 2010;12:1857–60.
7. Szilágyi IM, et al. Programming nanostructured soft biological surfaces by atomic layer deposition. Nanotechnology. 2013;24:24.
8. Lublóy É, Kopecskó K, Balázs GL, Restás Á, Szilágyi IM. Improved fire resistance by using Portland-pozzolana or Portland-fly ash cements. J Therm Anal Calorim. 2017;129:925–36.
9. Bakos LP, Mensah J, László K, Igricz T, Szilágyi IM. Preparation and characterization of a nitrogen-doped mesoporous carbon aerogel and its polymer precursor. J Thermal Anal Calorim. 2018;134:933–9.
10. Szilágyi IM, Santala E, Heikkilä M, et al. Thermal study on electrospun polyvinylpyrrolidone/ammonium metatungstate nanofibers: optimising the annealing conditions for obtaining WO3 nanofibers. J Thermal Anal Calorim. 2010;105:73.
11. Lublóy É, Kopecskó K, Balázs GL, Szilágyi IM, Madarász J. Improved fire resistance by using slag cements. J Therm Anal Calorim. 2016;125:271–9.
12. Jouybari HJ, Saedodin S, Zamzamian A, Nimvari ME, Wongwises S. Effects of porous material and nanoparticles on the thermal performance of a flat plate solar collector: an experimental study. Renewable Energy. 2017;114:1407–18.
13. Javaniyan Jouybari H, Saedodin S, Zamzamian A, Nimvari ME. Experimental investigation of thermal performance and entropy generation of a flat-plate solar collector filled with porous media. Appl Thermal Eng. 2017;127:1506–17.
14. Mahdavi M, Sharifpur M, Meyer JP. Implementation of diffusion and electrostatic forces to produce a new slip velocity in the multiphase approach to nanofluids. Powder Technol. 2017;307:153–62. https://doi.org/10.1016/j.powtec.2016.11.032.
15. Mahdavi M, Sharifpur M, Meyer JP. CFD modelling of heat transfer and pressure drops for nanofluids through vertical tubes in laminar flow by Lagrangian and Eulerian approaches. Int J Heat Mass Transf. 2015;88:803–13. https://doi.org/10.1016/j.ijheatmasstransfer.2015.04.112.
16. Mahdavi M, Garbadeen I, Sharifpur M, Ahmadi MH, Meyer JP. Study of particle migration and deposition in mixed convective pipe flow of nanofluids at different inclination angles. J Therm Anal Calorim. 2018. https://doi.org/10.1007/s10973-018-7720-y.
17. Ghasemi A, Dardel M, Ghasemi MH. Collective effect of fluid's coriolis force and nanoscale's parameter on instability pattern and vibration characteristic of fluid-conveying carbon nanotubes. J Pressure Vessel Technol. 2015;137:031301.
18. Mahdavi M, Sharifpur M, Ghodsinezhad H, Meyer JP. A new combination of nanoparticles mass diffusion flux and slip mechanism approaches with electrostatic forces in a natural convective cavity flow. Int J Heat Mass Transf. 2017;106:980–8. https://doi.org/10.1016/j.ijheatmasstransfer.2016.10.065.
19. Ghasemi A, Dardel M, Ghasemi MH, Barzegari MM. Analytical analysis of buckling and post-buckling of fluid conveying multi-walled carbon nanotubes. Appl Math Model. 2013;37:4972–92.
20. Wu C, et al. Multi-scale progressive failure mechanism and mechanical properties of nanofibrous polyurea aerogels. Soft Matter. 2018;14:7801–8.
21. Hoseinzadeh S, Ghasemiasl R, Bahari A, Ramezani AH. n-type WO3semiconductor as a cathode electrochromic material for ECD devices. J Mater Sci: Mater Electron. 2017;28:14446–52.
22. Hoseinzadeh S, Ghasemiasl R, Bahari A, Ramezani AH. The injection of Ag nanoparticles on surface of WO3 thin film: enhanced electrochromic coloration efficiency and switching response. J Mater Sci: Mater Electron. 2017;28:14855–63.

23. Ramezani AH, Hoseinzadeh S, Bahari A. The effects of nitrogen on structure, morphology and electrical resistance of tantalum by ion implantation method. J Inorg Organomet Polym Mater. 2018;28:847–53.
24. Yousef Nezhad ME, Hoseinzadeh S. Mathematical modelling and simulation of a solar water heater for an aviculture unit using MATLAB/SIMULINK. J Renew Sustain Energy. 2017;9:063702.
25. Hoseinzadeh S, Hadi Zakeri M, Shirkhani A, Chamkha AJ. Analysis of energy consumption improvements of a zero-energy building in a humid mountainous area. J Renew Sustain Energy. 2019;11:015103.
26. Hoseinzadeh S, Azadi R. Simulation and optimization of a solar-assisted heating and cooling system for a house in Northern of Iran. J Renew Sustain Energy. 2017;9:045101.
27. Hoseinzadeh S, Ghasemiasl R, Bahari A, Ramezani AH. Effect of post-annealing on the electrochromic properties of layer-by-layer arrangement FTO-WO3-Ag-WO3-Ag. J Electron Mater. 2018;47:3552–9.
28. Chamkha AJ. Hydromagnetic natural convection from an isothermal inclined surface adjacent to a thermally stratified porous medium. Int J Eng Sci. 1997;35:975–86.
29. Menni Y, Azzi A, Chamkha A. Enhancement of convective heat transfer in smooth air channels with wall-mounted obstacles in the flow path: a review. J Thermal Anal Calorim. 2018; 1–26.
30. Selimefendigil F, Oztop HF, Chamkha AJ. MHD mixed convection in a nanofluid filled vertical lid-driven cavity having a flexible fin attached to its upper wall. J Thermal Anal Calorim. 2018. https://doi.org/10.1007/s10973-018-7036-y.
31. Selimefendigil F, Oztop HF, Chamkha AJ. Natural convection in a CuO–water nanofluid filled cavity under the effect of an inclined magnetic field and phase change material (PCM) attached to its vertical wall. J Thermal Anal Calorim. 2018. https://doi.org/10.1007/s10973-018-7714-9.
32. Abedini A, Armaghani T, Chamkha AJ. MHD free convection heat transfer of a water–Fe_3O_4 nanofluid in a baffled C-shaped enclosure. J Therm Anal Calorim. 2019;135:685–95.
33. Dogonchi AS, Chamkha AJ, Ganji DD. A numerical investigation of magneto-hydrodynamic natural convection of Cu–water nanofluid in a wavy cavity using CVFEM. J Therm Anal Calorim. 2019;135:2599–611.
34. Chamkha AJ, Rashad AM, Armaghani T, Mansour MA. Effects of partial slip on entropy generation and MHD combined convection in a lid-driven porous enclosure saturated with a Cu–water nanofluid. J Therm Anal Calorim. 2018;132:1291–306.
35. Alsabery AI, Chamkha AJ, Saleh H, Hashim I. Natural convection flow of a nanofluid in an inclined square enclosure partially filled with a porous medium. Sci Rep. 2017. https://doi.org/10.1038/s41598-017-02241-x.
36. Sheikholeslami M, Ganji DD. Applications of nanofluid for heat transfer enhancement. New York: Elsevier; 2017.
37. Sheikholeslami M, Gorji-Bandpy M, Ganji DD. Lattice Boltzmann method for MHD natural convection heat transfer using nanofluid. Powder Technol. 2014;254:82–93.
38. Sheikholeslami M, Ganji DD. Nanofluid hydrothermal behavior in existence of Lorentz forces considering Joule heating effect. J Mol Liq. 2016;224:526–37.
39. Sheikholeslami M, Ganji DD, Rashidi MM. Magnetic field effect on unsteady nanofluid flow and heat transfer using Buongiorno model. J Magn Magn Mater. 2016;416:164–73.
40. Sheikholeslami M, Ganji DD. Nanofluid flow and heat transfer between parallel plates considering Brownian motion using DTM. Comput Methods Appl Mech Eng. 2015;283:651–63.
41. Sheikholeslami M, Ganji DD. Heat transfer of Cu-water nanofluid flow between parallel plates. Powder Technol. 2013;235:873–9.
42. Sheikholeslami M, Ganji DD. Analytical investigation for Lorentz forces effect on nanofluid Marangoni boundary layer hydrothermal behavior using HAM. Indian J Phys. 2017;91:1581–7.
43. Sheikholeslami M, Ashorynejad HR, Ganji DD, Yldrm A. Homotopy perturbation method for three-dimensional problem of condensation film on inclined rotating disk. Scientia Iranica. 2012;19:437–42.
44. Sheikholeslami M, Ganji DD, Ashorynejad HR. Investigation of squeezing unsteady nanofluid flow using ADM. Powder Technol. 2013;239:259–65.
45. Sheikholeslami M, Ganji DD. Magnetohydrodynamic flow in a permeable channel filled with nanofluid. Scientia Iranica. 2014;21:203–12.
46. Sheikholeslami M, Ganji DD. Transportation of MHD nanofluid free convection in a porous semi annulus using numerical approach. Chem Phys Lett. 2017;669:202–10.
47. Sheikholeslami M, Ashorynejad HR, Ganji D, Rashidi M. Heat and mass transfer of a micropolar fluid in a porous channel. Commun Numer Anal. 2014;2014:1–20.
48. Sheikholeslami M, Ziabakhsh Z, Ganji DD. Transport of magnetohydrodynamic nanofluid in a porous media. Colloids Surf, A. 2017;520:201–12.
49. Sheikholeslami M, Haq RU, Shafee A, Li Z. Heat transfer behavior of nanoparticle enhanced PCM solidification through an enclosure with V shaped fins. Int J Heat Mass Transfer. 2019;130:1322–42.
50. Sheikholeslami M. New computational approach for exergy and entropy analysis of nanofluid under the impact of Lorentz force through a porous media. Comput Methods Appl Mech Eng. 2019;344:319–33.
51. Sheikholeslami M. Numerical approach for MHD Al[Formula presented]O[Formula presented]-water nanofluid transportation inside a permeable medium using innovative computer method. Comput Methods Appl Mech Eng. 2019;344:306–18.
52. Sheikholeslami M, Gerdroodbary MB, Moradi R, Shafee A, Li Z. Application of Neural Network for estimation of heat transfer treatment of Al[Formula presented]O[Formula presented]-H[Formula presented]O nanofluid through a channel. Comput Methods Appl Mech Eng. 2019;344:1–12.
53. Sheikholeslami M, Mahian O. Enhancement of PCM solidification using inorganic nanoparticles and an external magnetic field with application in energy storage systems. J Clean Prod. 2019;215:963–77.
54. Nematpour Keshteli A, Sheikholeslami M. Nanoparticle enhanced PCM applications for intensification of thermal performance in building: a review. J Mol Liq. 2019;274:516–33.
55. Sheikholeslami M, Sadoughi MK. Simulation of CuO-water nanofluid heat transfer enhancement in presence of melting surface. Int J Heat Mass Transf. 2018;116:909–19.
56. Sheikholeslami M, Rokni HB. Numerical modeling of nanofluid natural convection in a semi annulus in existence of Lorentz force. Comput Methods Appl Mech Eng. 2017;317:419–30.
57. Sheikholeslami M, Seyednezhad M. Simulation of nanofluid flow and natural convection in a porous media under the influence of electric field using CVFEM. Int J Heat Mass Transf. 2018;120:772–81.
58. Sheikholeslami M, Rokni HB. Numerical simulation for impact of Coulomb force on nanofluid heat transfer in a porous enclosure in presence of thermal radiation. Int J Heat Mass Transf. 2018;118:823–31.
59. Sheikholeslami M, Shehzad SA. Numerical analysis of Fe3O4–H2O nanofluid flow in permeable media under the effect of external magnetic source. Int J Heat Mass Transf. 2018;118:182–92.

60. Sheikholeslami M, Zeeshan A. Analysis of flow and heat transfer in water based nanofluid due to magnetic field in a porous enclosure with constant heat flux using CVFEM. Comput Methods Appl Mech Eng. 2017;320:68–81.
61. Sheikholeslami M, Shehzad SA. Simulation of water based nanofluid convective flow inside a porous enclosure via non-equilibrium model. Int J Heat Mass Transf. 2018;120:1200–12.
62. Sheikholeslami M, Shehzad SA. Magnetohydrodynamic nanofluid convective flow in a porous enclosure by means of LBM. Int J Heat Mass Transf. 2017;113:796–805.
63. Sheikholeslami M, Shamlooei M. Fe3O4–H2O nanofluid natural convection in presence of thermal radiation. Int J Hydrogen Energy. 2017;42:5708–18.
64. Sheikholeslami M. Application of Darcy law for nanofluid flow in a porous cavity under the impact of Lorentz forces. J Mol Liq. 2018;266:495–503.
65. Sheikholeslami M, Jafaryar M, Li Z. Second law analysis for nanofluid turbulent flow inside a circular duct in presence of twisted tape turbulators. J Mol Liq. 2018;263:489–500.
66. Sheikholeslami M. Influence of magnetic field on Al_2O_3-H_2O nanofluid forced convection heat transfer in a porous lid driven cavity with hot sphere obstacle by means of LBM. J Mol Liq. 2018;263:472–88.
67. Sheikholeslami M. Solidification of NEPCM under the effect of magnetic field in a porous thermal energy storage enclosure using CuO nanoparticles. J Mol Liq. 2018;263:303–15.
68. Sheikholeslami M, Shehzad SA, Li Z, Shafee A. Numerical modeling for alumina nanofluid magnetohydrodynamic convective heat transfer in a permeable medium using Darcy law. Int J Heat Mass Transf. 2018;127:614–22.
69. Sheikholeslami M, Zeeshan A. Analysis of flow and heat transfer in water based nanofluid due to magnetic field in a porous enclosure with constant heat flux using CVFEM. Comput Methods Appl Mech Eng. 2017;320:68–81.
70. Li Z, Sheikholeslami M, Shafee A, Saleem S, Chamkha AJ. Effect of dispersing nanoparticles on solidification process in existence of Lorenz forces in a permeable media. J Mol Liq. 2018;266:181–93.
71. Sheikholeslami M. CuO-water nanofluid free convection in a porous cavity considering Darcy law. Eur Phys J Plus. 2017. https://doi.org/10.1140/epjp/i2017-11330-3.
72. Sheikholeslami M, Rokni HB. Magnetic nanofluid flow and convective heat transfer in a porous cavity considering Brownian motion effects. Phys Fluids. 2018;30:012003.
73. Sheikholeslami M, Chamkha AJ. Influence of Lorentz forces on nanofluid forced convection considering Marangoni convection. J Mol Liq. 2017;225:750–7.
74. Sheikholeslami M, Hayat T, Alsaedi A. Numerical simulation of nanofluid forced convection heat transfer improvement in existence of magnetic field using lattice Boltzmann method. Int J Heat Mass Transf. 2017;108:1870–83.
75. Hosseinzadeh S, Ostadhossein R, Mirshahvalad HR, Seraj J. Using simpler algorithm for cavity flow problem. Int J (MECHATROJ). 2017;1(1).
76. Hoseinzadeh S, Ghasemiasl R, Havaei D, Chamkha AJ. Numerical investigation of rectangular thermal energy storage units with multiple phase change materials. J Mol Liq. 2018;271:655–60.
77. Hoseinzadeh S, Moafi A, Shirkhani A, Chamkha AJ. Numerical validation heat transfer of rectangular cross-section porous fins. J Thermophys Heat Transfer. 2019; 1–7.
78. Yari A, Hosseinzadeh S, Galogahi MR. Two-dimensional numerical simulation of the combined heat transfer in channel flow. Int J Recent Adv Mech Eng. 2014;3:55–67.
79. Hoseinzadeh S, Sahebi SAR, Ghasemiasl R, Majidian AR. Experimental analysis to improving thermosyphon (TPCT) thermal efficiency using nanoparticles/based fluids (water). Eur Phys J Plus. 2017;132:20. https://doi.org/10.1140/epjp/i2017-11455-3.
80. Yari A, Hosseinzadeh S, Golneshan AA, Ghasemiasl R. Numerical simulation for thermal design of a gas water heater with turbulent combined convection. In: ASME/JSME/KSME 2015 Joint Fluids Engineering Conference, AJKFluids 2015; 2015. Vol. 1.